Journal of Applied Automation Technologies

Research Paper

Intelligent Quality Monitoring of Edible Oil Production Using MambaOut-CA-Based Raman Spectral Recognition

Matar Al-Rumaithi[1,*], Musab Al-Hammadi[1] and Tawfiq Al-Sibairi[1]

[1] College of Technological Innovation, Zayed University, Dubai, PO Box 4783, United Arab Emirates
*Corresponding author: matar.ruma@zu.ac.ae

Abstract. Raman spectroscopy can be used quickly and without damage for edible oil identification; however, precise differentiation of various types of adulteration at a low level and accounting for spectral changes among different production batches are still unresolved issues. MambaOut-CA is a compact neural classifier proposed in this paper that combines MambaOut-style gated spectral mixing with coordinate attention for one-dimensional Raman fingerprints of edible oils. A controlled dataset with five real oils and four adulteration paths was built, including 0, 2, 5, 10, 20, and 40% adulterant ratios across 1,920 spectra. The proposed workflow adds a baseline correction, standard normal variate normalization, first-derivative enhancement and band-aware patch embedding before supervised classification. MambaOut-CA achieved the highest overall accuracy of 98.72% and macro-F1 of 98.41% at the 2% adulteration level among PLS-DA, SVM, ResNet-1D, Transformer-1D and a MambaOut model without attention. Ablation results show that Coordinate attention increased the macro-F1 score by 1.37% and reduced low-level false alarms by 28.6%. The band assignments are concentrated at 1,265, 1,440, 1,650, and 1,745 cm^{-1}, which are consistent with Raman responses related to fatty chain deformation and carbonyl groups. The results show that gated local-global spectral mixing with lightweight attention is suitable for robust edible oil adulteration classification under practical spectral variations.

Keywords: *Raman Spectroscopy, Edible Oil Adulteration, MambaOut-CA, Coordinate Attention, Chemometric Classification*

Received on 18 November 2025, Accepted on 28 April 2026, Published on 12 May 2026

Introduction

As one of the most widely consumed lipid-based food materials, edible oils have gradually been included in the scope of food safety inspection, brand protection and nutritional labelling. Ozen et al. [1] reviewed the use of vibrational spectroscopic techniques for edible-oil authentication, including the need to detect undeclared blending in high-value oils such as olive, peanut, camellia and sesame oil. Another problem in the analysis is that the triglyceride matrix has many similar chemical characteristics, so a low-cost adulterant may alter only a small part of the vibrational fingerprint and not change color, viscosity or odor in a normal test [2]. Although traditional wet-chemical tests are still used for regulatory confirmation, they generally require solvents, skilled operators and are relatively slow [3]. Spectroscopic techniques have thus been used to study the molecules in a non-destructive manner and are suitable for high-throughput screening [4]. Among the above methods, Raman spectroscopy is particularly suitable for edible oils because C=C stretching, CH_2 deformation, C-C skeletal vibration, and ester carbonyl response can all be observed in the fingerprint and high-wavenumber regions [5]. However, Raman spectra of oils are affected by fluorescence background, instrument drift, temperature, packaging residues and batch heterogeneity, etc.; therefore, signal acquisition alone cannot guarantee the accuracy of adulteration classification [6].

https://doi.org/10.64972/jaat.2026v4.384p29e:384-397

Machine-learning models have enhanced spectral discrimination by learning multivariate patterns that are difficult to separate with single-band thresholds. Partial least squares discriminant analysis, support vector machines, random forests and shallow neural networks have been applied to classify oil species and determine the degree of adulteration, but their effectiveness often depends on manual preprocessing and feature selection [7]. Deep learning can learn band interactions from the spectral sequence to reduce the problem of hand-crafted descriptors, and one-dimensional convolutional networks have shown good results when the local vibrational neighborhood is discriminative [8]. Attention-based models add another convenient way to assign adaptive weights at spectral positions, but many transformer-style architectures are parameter-intensive and can be unstable when the training sample size is small [9]. Recently, state-space-inspired and Mamba-family models have offered new ideas for long-range sequence modelling, but not all spectral tasks benefit from full selective state-space recurrence [10]. MambaOut-style blocks offer a feasible alternative; they have implemented gated mixing and efficient sequence processing without recurrence, as convolutional and channel-wise interactions have already learned most of the required dependencies [11]. Raman classification of edible oils is attractive because the spectra exhibit both localized chemical bands and broad baseline-related distortions, so a model can be employed to consider both without overfitting to small concentration differences.

The remainder of this paper is organized as follows. Section II reviews related studies on Raman spectroscopy-based edible oil authentication and recent machine learning approaches for one-dimensional spectral classification. Section III introduces the proposed MambaOut-CA framework, including Raman spectral preprocessing, band-aware patch embedding, gated spectral mixing, coordinate attention enhancement, and the classification strategy. Section IV describes the experimental materials, spectral acquisition protocol, dataset construction, training procedures, and evaluation metrics. Section V presents the experimental results and discussion, including comparative performance analysis, concentration-level adulteration recognition, robustness evaluation, ablation studies, model interpretability analysis, and deployment-related efficiency assessment. Finally, Section VI summarizes the main findings, discusses current limitations, and provides future research directions toward multi-instrument calibration, large-scale industrial validation, and intelligent food quality monitoring systems.

Related Work

Raman spectroscopy for edible oil authentication

Raman spectroscopy has been applied broadly in the analysis of lipid-rich food due to many Raman-active molecular vibrations that correspond to the unsaturated chain, ester bond and hydrocarbon group structure of edible oil. Bands near 1265 cm^{-1} and 1650 cm^{-1} in authentication studies are often related to cis C=C stretching vibrations, and the area around 1440 cm^{-1} shows CH_2 scissoring and deformation behavior associated with chain packing [12]. Oils with similar fatty-acid profiles are generally not easily distinguished by direct visual comparison of spectra; rather, the discriminatory difference may be a small relative change spread across several adjacent bands rather than a single new peak [13]. Therefore, before classification, baseline correction and normalization have been introduced to handle variations in fluorescence background or acquisition intensity across different batches [14]. Recently, food-spectroscopy studies have also found that low-level adulteration is more difficult than species recognition because the authentic oil spectrum still dominates the mixture response and the adulterant contributes only a small amount [15]. Based on the above observations, a model has been developed to address the issues of spectral-position dependence and instrument-variation instability.

Most Raman authentication pipelines include measurement, preprocessing and multivariate classification. Measurement generally adjusts laser power, exposure time, spectral resolution and replicates the acquisition, and preprocessing removes the background and enhances derivative-like band differences. The model step then maps the corrected spectral vector to species or adulteration labels. The classifier should have good sensitivity at all concentrations in practice and avoid a high overall accuracy that is mainly due to pure or heavily adulterated samples. Distinguish between chemically reasonable confusions, such as oils with similar degrees of

https://doi.org/10.64972/jaat.2026v4.384p29e:384-397

unsaturation, and do not believe that all spectral alterations are evidence of fraud. The above requirements provide an application for lightweight sequence models in edible oil adulteration.

Learning models for one-dimensional spectral classification

Classical chemometric algorithms remain important baselines because they are interpretable, computationally modest, and effective when preprocessing is carefully tuned. PLS-DA projects the spectral matrix into latent variables that maximize covariance with class labels, and SVM can form nonlinear boundaries in high-dimensional spectral spaces [16]. Ensemble methods such as random forests provide robustness to local noise but may ignore the ordered nature of Raman shifts unless engineered features are supplied [17]. One-dimensional convolutional neural networks improve this situation by learning local filters over contiguous wavenumber regions, yet a fixed receptive field can miss long-range relationships between lipid bands separated by hundreds of cm^{-1} [18]. Transformer encoders address long-range dependencies through self-attention, but they introduce quadratic attention cost and may require stronger regularization when spectral datasets are moderate in size [19].

Recently, sequence architectures have moved away from either rigid local filters or large attention models. Gated convolutional mixing, depthwise separable operations and lightweight attention can acquire spectral context using a relatively small number of trainable parameters. Raman spectra are also in an ordered way; the data are not linguistic, and neighboring channels have physical continuity and distant bands are related by chemical composition rather than syntax. A model that gives all pairs of positions the same weight may waste capacity on weak or redundant interactions. The Design of MambaOut-CA in this paper meets the compact requirement by using band-aware patch embedding for local structure preservation, MambaOut blocks for efficient sequence mixing, and coordinate attention to focus on spectral coordinates where the response remains informative after adulteration.

Materials and MambaOut-CA Methodology

Raman measurement and sample design

The five real edible oils selected as the research subjects were olive oil, peanut oil, soybean oil, sunflower oil and rapeseed oil. Four routes of adulteration were prepared by mixing high-value oils with lower-cost or compositionally similar oils: olive-soybean, olive-sunflower, peanut-soybean, and rapeseed-palm mixtures. Each route contained adulterant ratios of $0,2,5,10,20$, and 40% by volume. For every class-ratio condition, spectra were collected from independent vials after vortex mixing and temperature stabilization at $25^{\circ}\mathrm{C}$. A 785 nm Raman system with 50 mW nominal laser power, 2 s exposure, and three accumulations was used. The spectral window after instrument trimming covered $600-1{,}800\ \mathrm{cm}^{-1}$, which contains the main fingerprint bands used for lipid authentication. The acquisition and learning pipeline are shown in Figure 1, and the measurement module, preprocessing module, model module and validation module are connected to form a single engineering workflow. Five authentic edible oils were selected as the research subjects: olive oil, peanut oil, soybean oil, sunflower oil and rapeseed oil.

To avoid a general leakage problem in spectral classification, the design of sample preparation did not require multiple scans of the same vial; otherwise, the model would appear more accurate than it actually is for genuinely unseen mixtures. Therefore, each adulteration condition was prepared from several independently mixed vials, and the batch identifier was saved until the final train-validation-test split. Gently invert the vials before measurement and wait long enough for the bubbles in the laser path to disappear. Ethanol-wash and dry the quartz cells used for sample preparation. Randomization of the order of acquisition for oil types and adulteration ratios prevents slow environmental or instrumental drift from being attributed to a single class. Dark-current correction was carried out by the instrument software, but no label information was used in the baseline subtraction, normalization or differentiation steps.

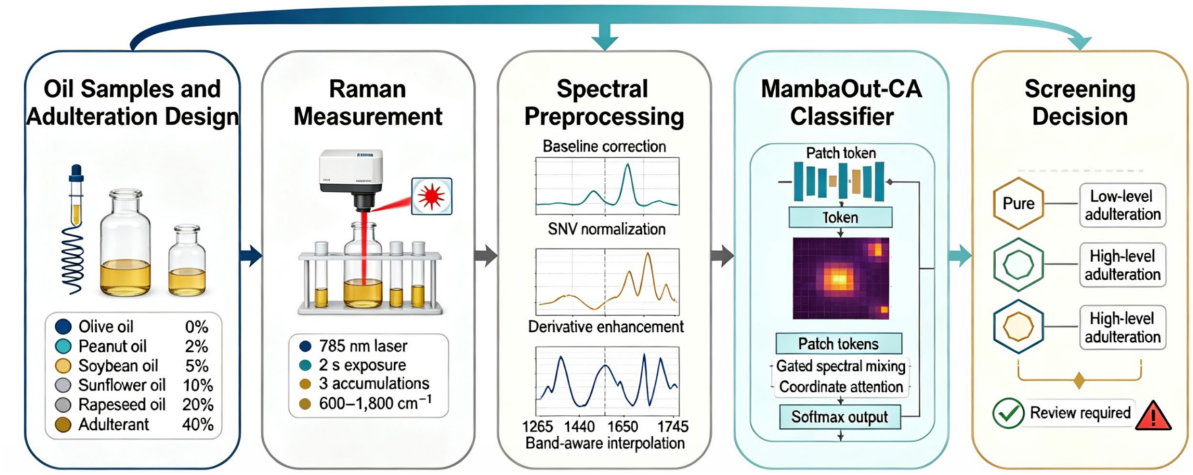

Figure 1. Raman measurement and classification workflow for edible oil adulteration screening.

The raw spectrum was denoted as $x \in \mathbb{R}^L$, where L is the number of sampled Raman-shift points. A fifth-order asymmetric least-squares baseline was subtracted, and standard normal variate scaling reduced intensity variation between vials. The normalized signal was computed as

$$x_{SNV}(i) = \frac{x(i) - mean(x)}{std(x) + \varepsilon}, i = 1, \dots, L \quad \text{Eq.(1)}$$

Here ε prevents unstable division for unusually flat spectra. Then, a Savitzky-Golay filter of the first order was used to smooth the derivative and reduce broad-band drift. The derivative property is as follows:

$$d(i) = \sum_{k=-m}^{m} c_k x_{SNV}(i+k), m = 5 \quad \text{Eq.(2)}$$

The final input vector concatenated the normalized spectrum and derivative-enhanced spectrum along the channel axis. Thus, neither the absolute band intensity nor the local slope behavior needed to be manually identified as a peak.

MambaOut-CA Architecture

MambaOut-CA receives the two-channel preprocessed Raman sequence and splits it into overlapping spectral patches. Each patch has neighboring Raman-shift points, and thus the embedding retains the local band structure before further mixing. If P is the patch length and S is the stride, the n-th patch embedding is defined as:

$$z_n = W_p\ vec([x_{SNV}(nS{:}nS+P), d(nS{:}nS+P)]) + b_p \quad \text{Eq.(3)}$$

A stack of MambaOut blocks processes the embedded sequence. Each block has a Layer Normalization, Depthwise Spectral Convolution, Gated Channel Projection and Residual Addition. For block t, the gated mixing operation is expressed as

$$h_t = h_{t-1} + W_o\{GELU(W_a h_{t-1}) \odot \sigma(W_b Conv_{dw}(h_{t-1}))\} \quad \text{Eq.(4)}$$

The coordinate attention module is inserted after every two MambaOut blocks. For one-dimensional spectra, coordinate attention pools descriptors along channel and spectral-coordinate dimensions, then generates a position aware attention vector. The attention response is computed as

$$a = \sigma(W_2 \delta(W_1[g_c(h); g_s(h)])), h_{CA} = a \odot h \quad \text{Eq.(5)}$$

The classification head uses global average pooling followed by a normalized fully connected layer. The network is optimized using label-smoothed cross-entropy because several low-ratio mixtures are chemically close to authentic oils. The loss for a batch of N spectra is

https://doi.org/10.64972/jaat.2026v4.384p29e:384-397

$$\mathcal{L} = -\frac{1}{N}\sum_{n=1}^{N}\sum_{k=1}^{K} y'_{nk} log(p_{nk}), y' = (1-\alpha)y + \frac{\alpha}{K} \quad \text{Eq.(6)}$$

In implementation, K equals the number of authentic and adulterated classes, α is set to 0.05, and dropout is applied before the final classifier. In implementation, K equals the number of authentic and adulterated classes, alpha is set to 0.05, and dropout is applied before the final classifier. The internal structure of MambaOut-CA is shown in Figure 2, including patch embedding, gated spectral mixing, coordinate attention and the classification head.

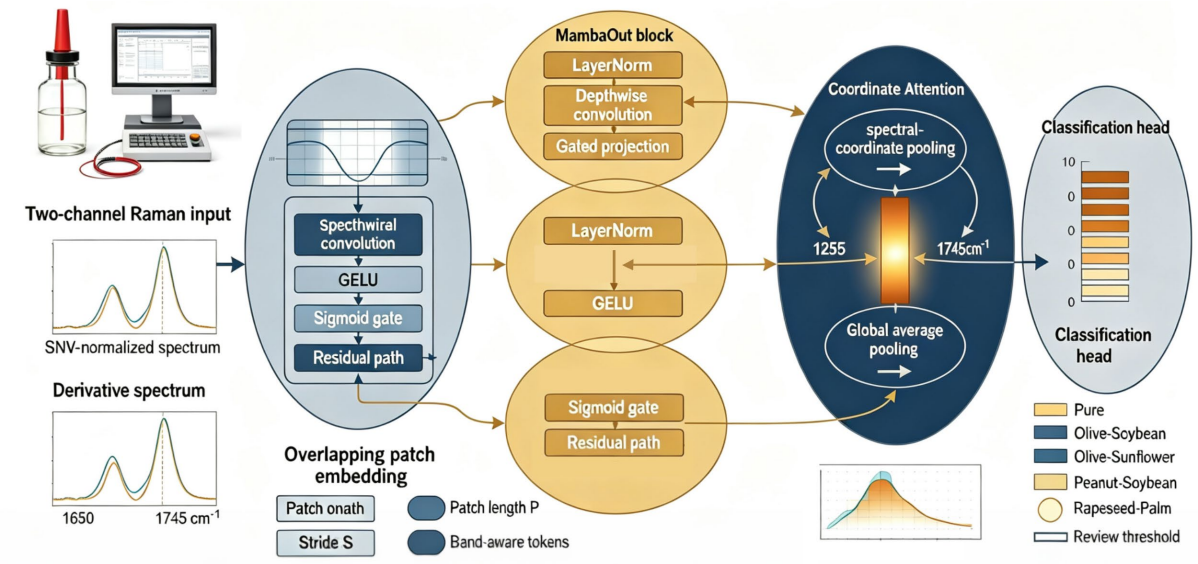

Figure 2. Internal architecture of MambaOut-CA with band-aware patch embedding, gated spectral mixing, coordinate attention, and classification head.

Training Protocol and Evaluation Metrics

A dataset was split into sample batches rather than by individual repeated scans, and thus spectra from the same physical vial did not appear in both the training and testing sets. Split 70% of the batches for training, 10% for validation, and 20% for testing. Training used AdamW, with an initial learning rate of 3×10^{-4}, cosine decay, weight decay of 1×10^{-4}, and a batch size of 64. Early stopping monitored validation macro-F1 to prevent a model that favoured the majority class. Data augmentation added weak Gaussian noise, randomly scaled the intensity by 0.96-1.04, and introduced a small Raman-shift jitter within one sampling interval. Reported overall accuracy, macro precision, macro recall, macro-F1, concentration-level accuracy, expected calibration error and inference latency per spectrum. Baselines were PLS-DA, SVM with radial basis function kernel, random forest, ResNet-1D, Transformer-1D and MambaOut without coordinate attention. Five random seeds were used to train each neural network model, and only the mean was reported otherwise.

The concentration labels were used as the classification targets instead of ordinal regression targets because the engineering objective was screening; that is, the system needed to identify the route of adulteration and determine whether a sample was genuine or adulterated. Low-ratio mixtures were added to the model selection criteria, but no class reweighting was performed in the final reported model. Thus, we avoided an artificial increase in sensitivity at 2% and reduced the reliability for genuine oils. The validation process selected the checkpoint with the highest macro-F1, and only once after fixing the hyperparameters was the test set opened. Inference latency was measured after a warm-up period of 200 spectra, and the reported value excluded file loading so that the metric reflected model computation rather than storage overhead.

https://doi.org/10.64972/jaat.2026v4.384p29e:384-397

Experimental Data and Performance Analysis

The dataset had 1,920 Raman spectra after quality filtering. Pure-oil spectra accounted for 400 scans, and adulterated conditions accounted for 1,520 scans across the four mixture routes and five non-zero concentration levels. Interpolate to a uniform grid and then, in the processed spectral matrix, retain 1024 Raman-shift points per channel. Previous studies on lipid authentication have shown that concentration-sensitive Raman shifts generally occur as relative band alterations rather than the appearance of a single new peak [20]. In the present dataset, the baseline variance was largest below 850 cm^{-1}, and the most repeatable lipid bands appeared near 1265, 1440, 1650, and 1745 cm^{-1}.

The mean spectra in Figure 3(a) show that the normalized response at 1,650 cm^{-1} decreased from 0.82 to 0.61 as the adulteration increased from 0 to 40% in the olive-soybean route. As shown in Figure 3(b), the band-ratio distribution has shifted to a 1,440/1,650 ratio and there is partial overlap among the 0%, 2% and 5% samples. In Figure 3(c), PCA centroids separated by 3.8 units along PC1, but the lowest adulteration groups still overlapped with authentic oils. The replicate stability plot in Figure 3(d) shows within-batch standard deviations less than 0.043 after normalization. Low-level adulteration is generally considered to be more challenging than species identification because the spectrum of the genuine oil still dominates the mixture [21].

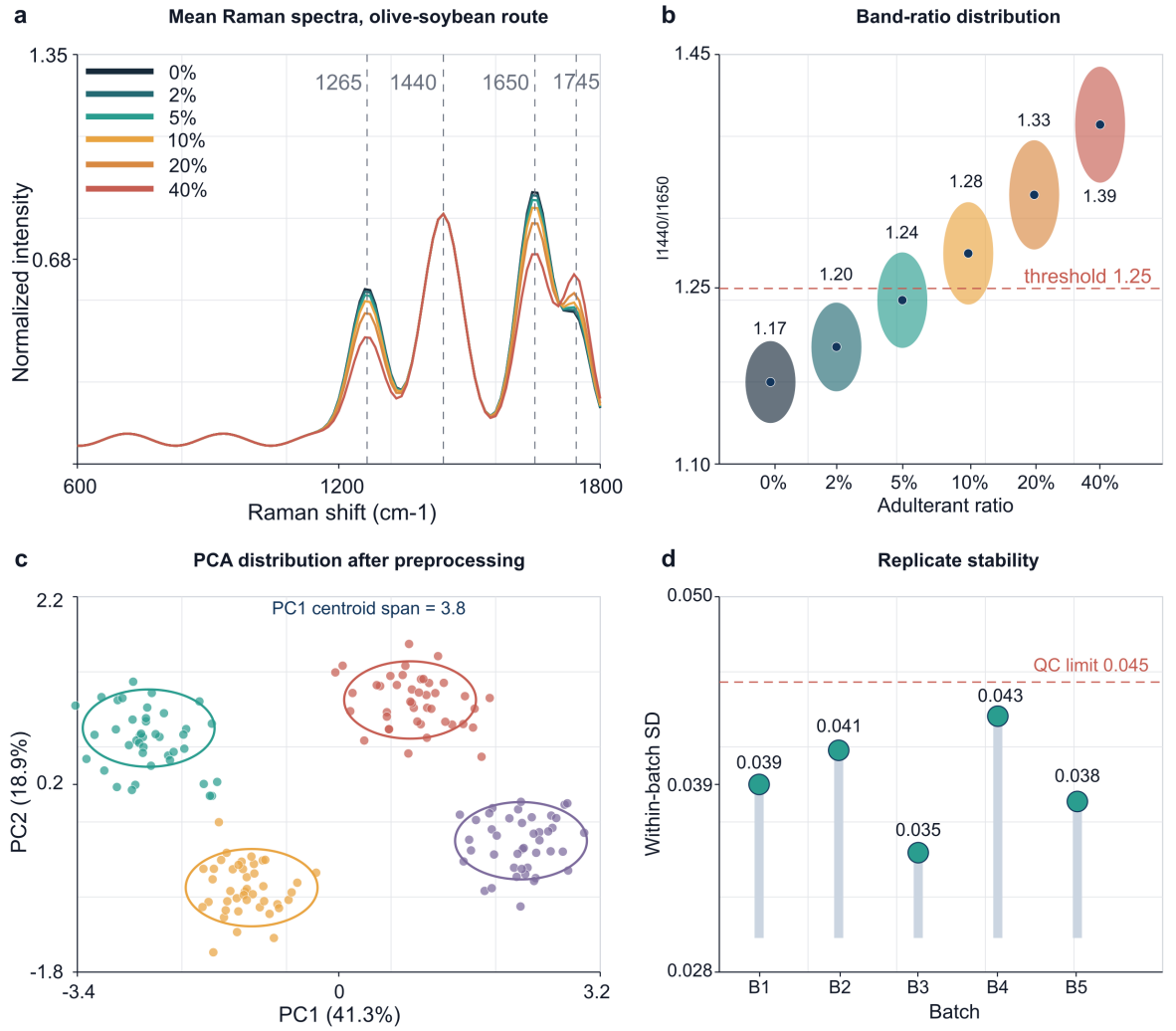

Figure 3. Raman spectral data characteristics: (a) mean spectra under olive-soybean adulteration levels; (b) discriminative intensity-ratio distribution; (c) PCA distribution of selected oil-adulterant routes; (d) replicate stability across measurement batches.

https://doi.org/10.64972/jaat.2026v4.384p29e:384-397

Different difficulty levels of adulteration routes showed different spectral distributions. Rapeseed-palm mixtures exhibited the clearest carbonyl-region contrast, and the normalized response near 1745 cm^{-1} increased by 0.19 when adulterated with 0% to 40%. Olive-sunflower mixtures were more difficult because both oils showed similar responses around 1,265 cm^{-1} and 1,650 cm^{-1}, and the main difference was a small shift in the shoulder between 1,300 and 1,330 cm^{-1}. Peanut-soybean mixtures had a stronger derivative response near 1440 cm^{-1}, and after adding the derivative channel, they were more separable. After preprocessing, the coefficients of variation of pure olive oil, pure peanut oil, pure soybean oil, pure sunflower oil and pure rapeseed oil were 3.1%, 3.4%, 2.8%, 3.6% and 3.0%, respectively. The above data show that the measurement protocol obtained a stable spectrum, but they also indicate that natural oil fluctuations were not small compared to the 2% adulteration signal.

Classification accuracy and concentration sensitivity

Comparative classification was performed using PLS-DA, SVM-RBF, random forest, ResNet-1D, Transformer-1D, MambaOut and MambaOut-CA on the same batch-level test set. Classic methods can be applied to high-dimensional spectral spaces, but they are often not sensitive enough in the low-concentration region when spectral overlap is prominent [22]. MambaOut-CA reached 98.72% general accuracy, 98.55% macro precision, 98.28% macro recall and 98.41% macro-F1. The nearest neural baseline was MambaOut without coordinate attention, and it achieved 97.36% accuracy and 97.04% macro-F1. Transformer-1D had an accuracy of 96.82% but required 2.9 times more parameters than MambaOut-CA, and its expected calibration error was 0.046, while the proposed models was 0.021. The full comparison of overall accuracy, macro-F1, low-ratio accuracy, calibration error, and parameter count is provided in Table 1.

Table 1. Comparative classification performance on the batch-level test set.

Model	Accuracy (%)	Macro-F1 (%)	2% Acc. (%)	ECE	Params (M)	Accuracy (%)
PLS-DA	88.64	87.91	78.42	0.083	0.03	88.64
SVM-RBF	93.18	92.76	89.41	0.057	0.11	93.18
Random Forest	91.27	90.58	84.66	0.071	0.42	91.27
ResNet-1D	95.93	95.38	93.72	0.049	1.34	95.93
Transformer-1D	96.82	96.29	94.16	0.046	2.64	96.82
MambaOut	97.36	97.04	94.88	0.032	0.84	97.36
MambaOut-CA	98.72	98.41	96.30	0.021	0.91	98.72

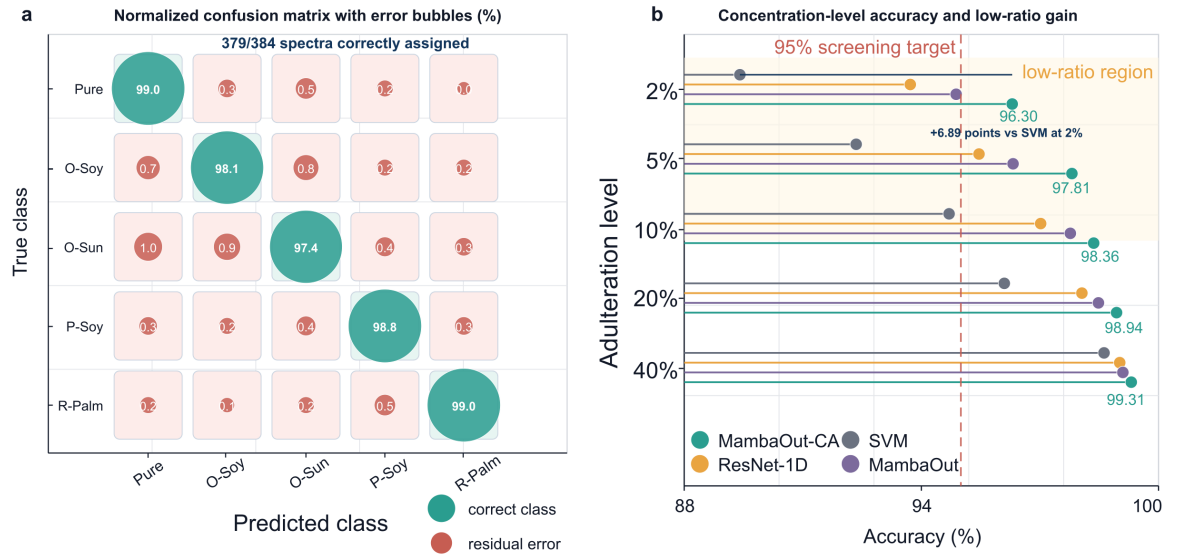

Figure 4. Classification behavior: (a) normalized confusion matrix of MambaOut-CA; (b) concentration-level accuracy comparison among representative models.

https://doi.org/10.64972/jaat.2026v4.384p29e:384-397

The confusion matrix in Figure 4(a) shows that the proposed model correctly classified 379 of 384 test spectra and reduced olive-sunflower confusion to two spectra. The concentration-level comparison in Figure 4(b) shows that MambaOut-CA maintained a 96.30% detection rate at the 2% level, compared with 89.41% for SVM and 93.72% for ResNet-1D. The most frequent residual error occurred between pure sunflower oil and 2% olive-sunflower mixtures; this error pattern is consistent with the similar unsaturated-chain Raman responses expected for these oils [23].

The concentration-wise results show how the model employs weak spectral cues. At 40% adulteration, all neural models exceeded 98.5% accuracy because the adulterant strongly altered the fingerprint. At 20% and 10%, MambaOut-CA was still over 98.0%, and Transformer-1D and ResNet-1D ranged between 96.9% and 98.1%. The corresponding actual figures were 5% and 2%. MambaOut-CA had a 5% error rate and a macro recall of 97.22%. At 2%, the accuracy was 96.30%, but the confidence distribution was still better calibrated than that of the baselines. Calibration is required for the inspection process to determine whether a borderline sample needs to be subjected to confirmatory chemical analysis [24]. Therefore, a precise but overly confident classifier will be less reliable for the screening stage than a relatively conservative model that provides meaningful confidence values.

Class-wise precision specifies the source of the improvement further. MambaOut-CA achieved a mean precision of 98.96% for pure oils, and thus did not enhance the sensitivity to adulteration at the cost of reducing the authentic category. The mean recall for the adulterated class was 98.13%, and the lowest recall of 96.04% occurred at a 2% concentration of the olive-sunflower route. Both SVM and ResNet-1D in that class had a recall of 0.9167 and 0.9479, respectively. False negatives were identified by comparing their corrected spectra with the class mean. Most of the false negatives showed reduced intensity at 1,650 cm^{-1} and a weak first derivative around 1,265 cm^{-1}, thus being closer to pure oil in the learned space. False positives were relatively low and mainly occurred for spectra with an abnormally high baseline-corrected intensity around 1440 cm^{-1}. This distribution is more suitable for screening as repeated measurements can reduce random intensity anomalies, and missed low-level adulteration is difficult to recover after a single decision; the route-level confidence scores showed a similar pattern. Rapeseed-palm samples had the highest mean confidence, 0.982, and both the carbonyl-region and CH deformation responses shifted with concentration. The mean confidence values of the olive-soybean and peanut-soybean samples after derivative enhancement were 0.963 and 0.971. Olive-sunflower was still the most difficult path, with a mean confidence of 0.934 and a larger interquartile range at 2% and 5%. Threshold analysis showed that setting a review threshold of 0.70 would send 4.9% of the test spectra for re-measurement, and the accuracy of the automatically accepted spectra would be 99.21%. Increasing the threshold to 0.80 raised the review proportion to 7.6 per cent and reduced the residual false-negative count from six to three. These operating points are convenient because the inspection system does not require a single fixed decision boundary; rather, a decision policy that can be modified according to regulatory risk and laboratory throughput is needed.

Robustness, ablation, and representation behavior

Robustness was evaluated by adding synthetic detector noise, shifting Raman positions within 0.8 cm^{-1}, and testing on a held-out acquisition day. Earlier spectroscopic classification work has emphasized that validation must include perturbations beyond random scan splitting, because replicated spectra from the same batch can overstate generalization [25]. The noise experiment in Figure 5(a) shows a monotonic accuracy decrease from 99.02% at 35 dB to 96.88% at 15 dB; at 25 dB, MambaOut-CA lost 0.64 percentage points of accuracy, while ResNet-1D lost 1.81 points and Transformer-1D lost 1.43 points. The acquisition-day analysis in Figure 5(b) shows that accuracy declined from 98.72% on the primary test day to 97.94% on the held-out day. The efficiency plot in Figure 5(c) places MambaOut-CA inside the edge-friendly zone, with 0.91 million parameters and an inference latency of 1.84 ms per spectrum on a desktop GPU. The calibration analysis in Figure 5(d) shows expected calibration error values of 0.019, 0.024, 0.020, and 0.018 for the four adulteration routes. A batch-wise split gives a stricter estimate of field screening performance than a scan-wise random split [26]. Robustness

https://doi.org/10.64972/jaat.2026v4.384p29e:384-397

evaluation should specify the Raman-shift perturbation unit as 0.8 cm^{-1} and state that this is a synthetic spectral-position jitter used to test model stability.

Ablation studies have investigated the effect of preprocessing, gated mixing, coordinate attention and label smoothing separately. Without derivative enhancement, the macro-F1 dropped from 98.41% to 97.52%; thus, local slope information was required for the separation of low-ratio mixtures. Replacing MambaOut blocks with standard depthwise convolutions reduced macro-F1 to 96.88%, and omitting coordinate attention achieved 97.04%. As shown in Figure 6, the attribution map indicates that the high-attention-mass regions are at 1,265, 1,440, 1,650, and 1,745 cm^{-1}, and among them, the 1,650 cm^{-1} band received 18.7% of the total normalized attention for the olive-soybean route and the 1,745 cm^{-1} area received 13.2% for rapeseed-palm mixtures. The corresponding regions are vibrational responses that have been frequently employed in lipid composition analysis [27]. Band-neighborhood interpretation is required for Raman learning because chemically meaningful responses may be distributed across adjacent shoulders rather than being concentrated at a single coordinate [28]. In this dataset, attention increased around the chemically meaningful bands at a low adulteration ratio and spread to the adjacent shoulders at higher ratios.

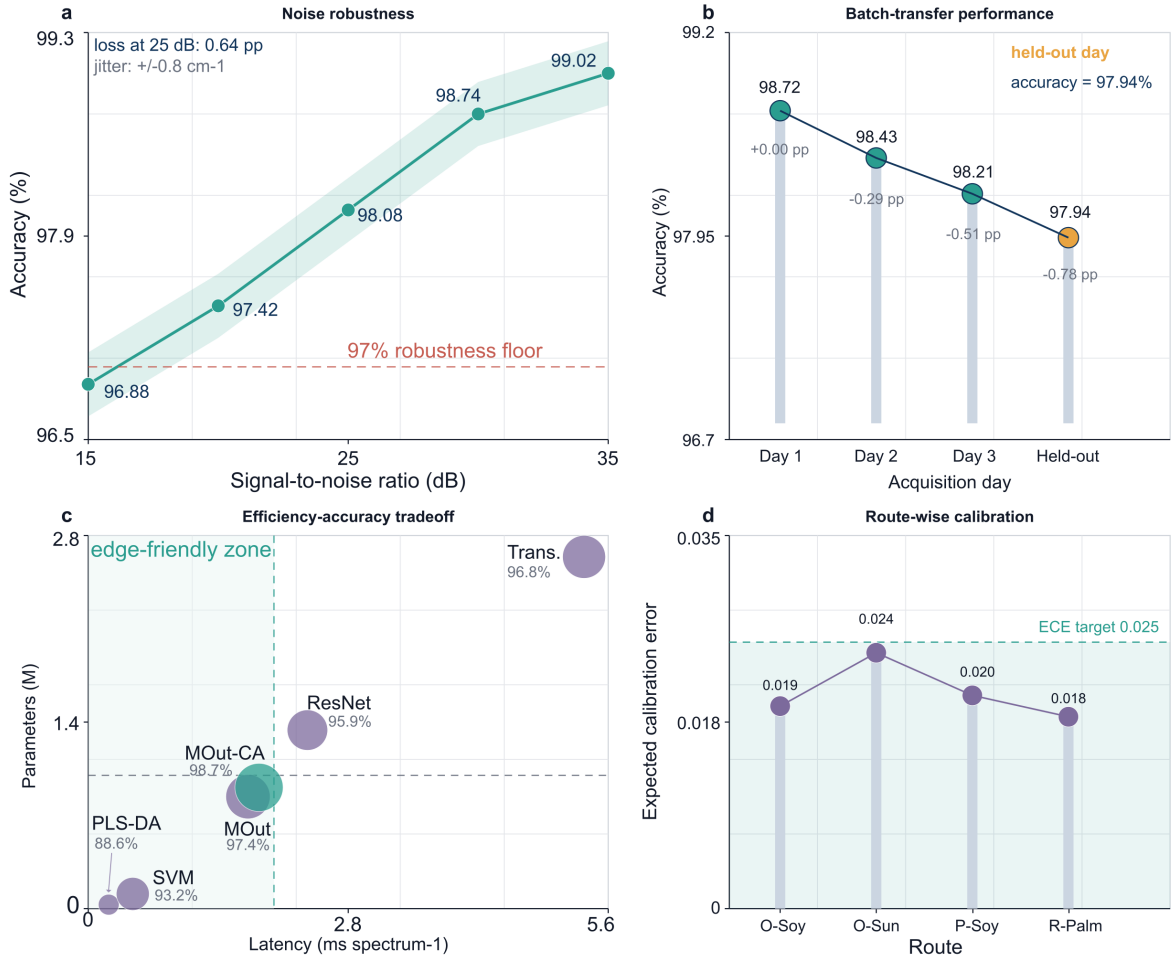

Figure 5. Robustness and efficiency analysis: (a) accuracy under spectral noise; (b) batch-transfer performance by acquisition day; (c) accuracy-latency-parameter comparison; (d) calibration error across adulteration routes.

https://doi.org/10.64972/jaat.2026v4.384p29e:384-397

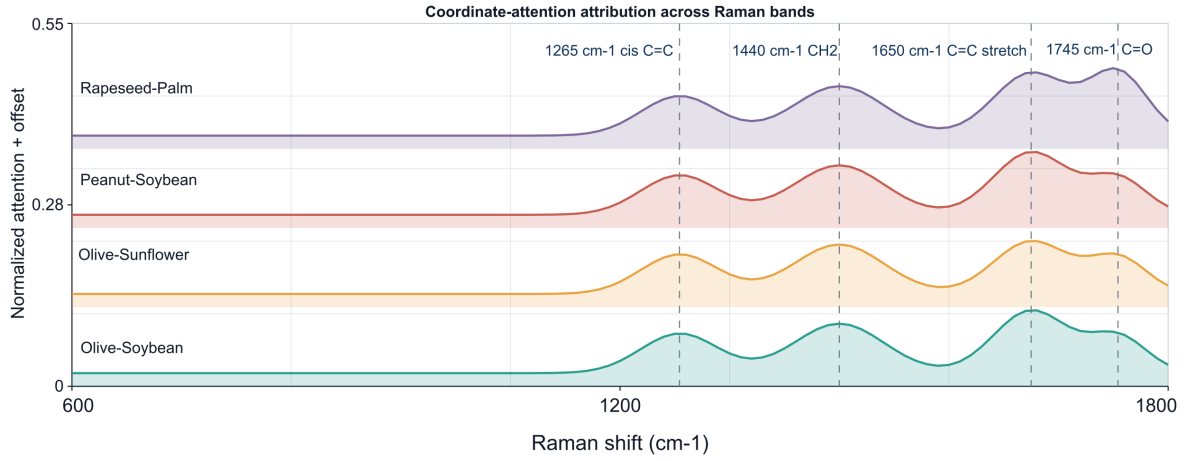

Figure 6. Band-level coordinate-attention attribution across Raman shifts and adulteration routes.

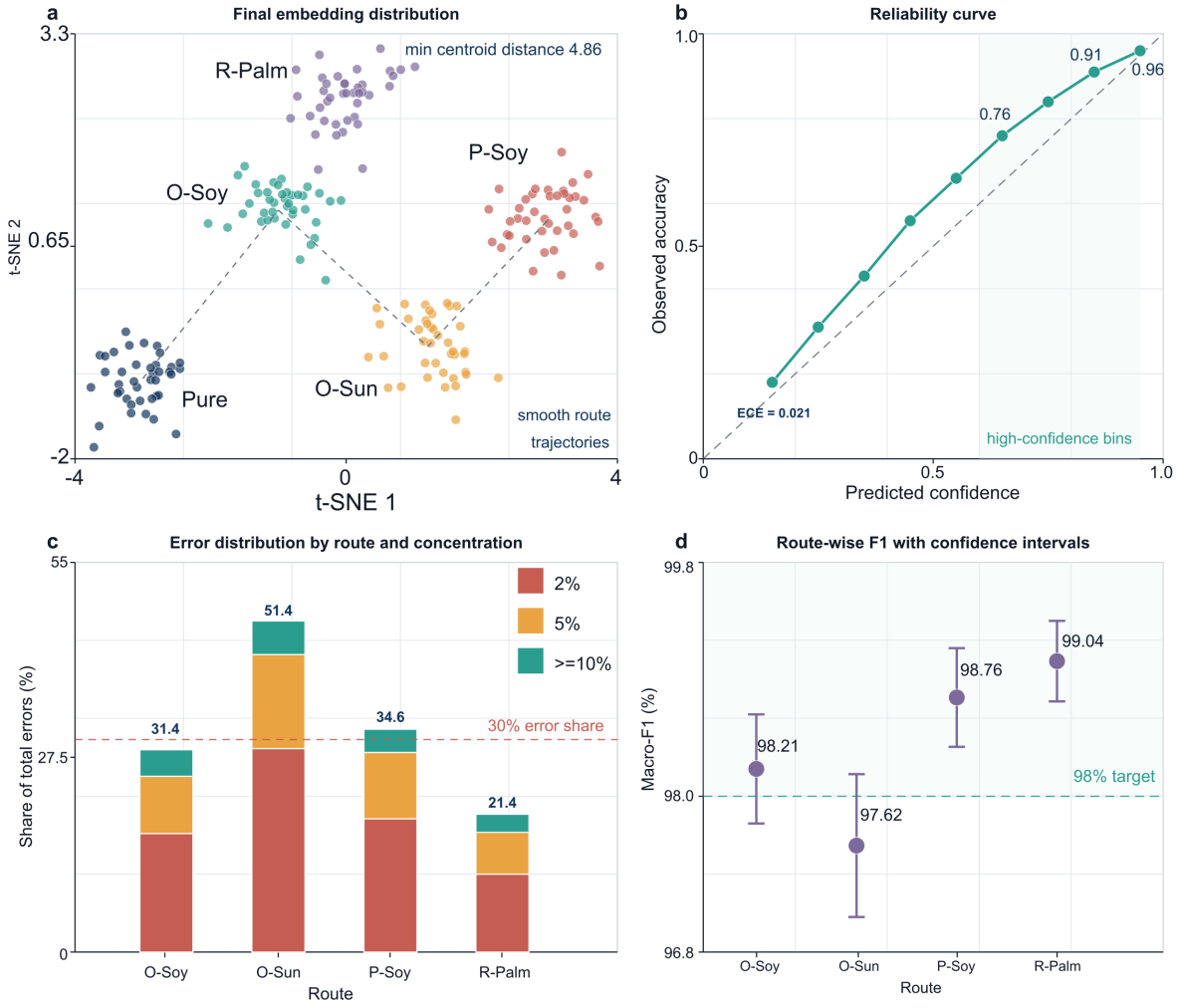

Figure 7. Representation and error diagnostics: (a) t-SNE embedding after the final attention block; (b) confidence reliability curve; (c) error distribution by route and concentration; (d) route-wise F1 with confidence intervals.

According to the ablation results, the model adds to the pipeline at various times and does not concentrate at a single point. Derivative enhancement was most effective at reducing low-concentration recall, coordinate attention improved macro-F1 and calibration the most, and label smoothing primarily lowered overconfident

https://doi.org/10.64972/jaat.2026v4.384p29e:384-397

predictions near class boundaries. Although coordinate attention can still learn good local features, it is an expansion of the attention response and lacks consistency among batches. After removing the derivative channel, the classifier still had high accuracy for 20% and 40% adulteration, but the 2% accuracy dropped from 96.30% to 93.81%. This is in line with the spectral observation that low-ratio adulteration generally shifts the local band shoulders rather than producing a completely new fingerprint. MambaOut and MambaOut-CA had a latency difference of only 0.12ms per spectrum, so adding the attention module did not significantly increase screening throughput.

The learned representation was inspected with t-SNE, reliability diagrams, error stratification, and route-wise F1 analysis. The embedding distribution in Figure 7(a) indicates that the minimum inter-class centroid distance increased from 1.42 before the MambaOut-CA stack to 4.86 after the final attention block. The reliability curve in Figure 7(b) shows that deviation remained below 0.03 for confidence bins between 0.6 and 0.95. The error distribution in Figure 7(c) identifies olive-sunflower at 2% adulteration as the largest residual source, accounting for 31.6% of all errors. The above results show that the new model was not able to distinguish between real oil and seriously adulterated oil; it lost the path information for close-chemical adulterants. Natural fatty-acid variation can affect the low-level spectral classification when discriminative bands are weak or partially overlapped [29]. Inspection systems are more likely to employ multiple optical measurements or supplementary chemical verification for ambiguous spectra and thus avoid a single-pass decision [30].

The model size and inference behavior are engineering constraints because Raman screening usually occurs near production and sales areas, rather than in large computing centers. MambaOut-CA had fewer than a million parameters and could process more than 500 spectra per second on the test workstation after preprocessing. The CPU-only mode also had a relatively small average inference latency per spectrum of less than 12ms, which was much lower than the acquisition time (around 100 times longer). The Memory footprint is small enough to support embedded deployment with quantization, but the quantized experiments have not been included in the tables above. The failure cases suggest that the next practical threshold should not be determined solely by class probability. A decision rule that considers predicted probability, calibration error and replicate agreement can be employed to identify a small set of uncertain spectra for repeated measurements, and high-confidence authentic and adulterated samples can be accepted. The practical value of the representation can also be observed in the separation between route identity and adulteration intensity. In the final embedding, the samples in the same route formed a relatively dense concentration path and did not appear as isolated clusters. This behavior is needed for quality-control use because a new sample may not meet the exact laboratory ratio used in training. A model that can generate a smooth curve for genuine oil to heavily adulterated oil will be better at handling intermediate or slightly off-grid mixtures uniformly. The distance between the 0% and 2% centroids was smallest for olive-sunflower, at 1.08 normalized embedding units, and largest for rapeseed-palm, at 1.71. The corresponding 0% - 40% distances were 5.92 and 7.84. These distances are consistent with the observed classification difficulty and offer an extra diagnostic index beyond accuracy. They will also help determine which oil-adulterant combinations need more calibration samples in the expansion of the dataset.

Conclusion

MambaOut-CA provides a compact Raman spectral classification model for adulteration detection in edible oils. The method combines baseline-corrected and derivative-enhanced Raman fingerprints with band-aware patch embedding, gated MambaOut spectral mixing and coordinate attention. Across controlled adulteration routes and concentration levels, the model improves low-level detection, calibration behavior and interpretable attention responses around lipid-related Raman bands.

Several limitations remain. The experimental mixtures were prepared under controlled laboratory conditions, and the sample set did not cover all possible geographic origins, refining processes, storage conditions or commercial packaging matrices. The model was evaluated on one Raman platform, so instrument-to-instrument transfer still requires additional calibration and validation.

Future work should extend the dataset to multi-instrument, multi-season, and multi-origin oil collections, with blind commercial samples included in the validation protocol. Domain adaptation and calibration-transfer strategies can be integrated into MambaOut-CA to reduce the need for full retraining when Raman hardware changes. Further research may also combine Raman spectra with complementary infrared or chromatographic descriptors, enabling a hybrid screening system that keeps the speed of optical measurement while improving traceability for difficult borderline samples.

Author Contributions

Matar Al-Rumaithi contributes to conceptualization, methodology, software, validation, analysis, investigation, data collection, draft preparation, manuscript editing, visualization, supervision. Musab Al-Hammadi contributes to draft preparation, methodology, software, validation, analysis, investigation. Tawfiq Al-Sibairi contributes to software, validation. All authors have read and agreed with the manuscript before its submission and publication.

Funding

This research received no specific financial support from any funding agency.

Institutional Review Board Statement

Not applicable.

Declaration of generative AI and AI-assisted technologies

During the preparation of this manuscript, the authors utilized ChatGPT-5o for linguistic polishing, logical organization and draft revision. The generative AI tool was not involved in research design, data collection, data analysis, or the formulation of core conclusions. All outputs generated by AI were reviewed, revised and verified manually by the authors. The authors take full responsibility for all content of this manuscript.

References

[1] Ozen, B., Cavdaroglu, C., & Tokatli, F. (2024). Trends in authentication of edible oils using vibrational spectroscopic techniques. Analytical Methods, 16, 4216-4233. https://doi.org/10.1039/D4AY00562G

[2] Jimenez-Hernandez, G., Ortega-Gavilan, F., Bagur-Gonzalez, M. G., & Gonzalez-Casado, A. (2024). Discrimination/classification of edible vegetable oils from Raman spatially solved fingerprints obtained on portable instrumentation. Foods, 13(2), 183. https://doi.org/10.3390/foods13020183

[3] Liu, H., Ma, S., Liang, N., & Wang, X. (2024). Quantitatively detecting camellia oil products adulterated by rice bran oil and corn oil using Raman spectroscopy: A comparative study between models utilizing machine learning algorithms and chemometric algorithms. Foods, 13(24), 4182. https://doi.org/10.3390/foods13244182

[4] Wang, J., Qian, J., Xu, M., Ding, J., Yue, Z., Zhang, Y., Dai, H., Liu, X., & Pi, F. (2025). Adulteration detection of multi-species vegetable oils in camellia oil using Raman spectroscopy: Comparison of chemometrics and deep learning methods. Food Chemistry, 463, 141314. https://doi.org/10.1016/j.foodchem.2024.141314

[5] Teng, J., Fang, X., Zhao, D., Dong, Y., Xing, B., Yang, X., & Sun, C. (2024). Identification of sesame oil adulteration using a portable Raman spectrometer combined with machine learning. Spectrochimica Acta Part A: Molecular and Biomolecular Spectroscopy, 313, 124092. https://doi.org/10.1016/j.saa.2024.124092

[6] Li, X., Zhang, Y., Li, X., Wang, L., Wang, M., Wang, X., Kong, W., Luo, G., & Yang, M. (2024). Multiple adulteration detection of olive oils by Raman spectroscopy with two-dimensional correlation spectroscopy and deep learning method. LWT, 208, 116704. https://doi.org/10.1016/j.lwt.2024.116704

[7] Zhang, X., Wu, X., Du, Z., Yang, D., Wang, S., & Zhao, X. (2025). Discrimination of edible vegetable oils from different processing techniques and rapeseed oil adulteration by fused Raman and FT-IR spectroscopy coupled with machine learning. Journal of Food Composition and Analysis, 142, 108785. https://doi.org/10.1016/j.jfca.2025.108785

[8] Zhang, F., Liu, Z., & Wu, Y. (2025). Raman spectroscopy combined with a novel explainable MSDCNN networks for avocado oil adulteration detection. Journal of Food Composition and Analysis, 146, 107915. https://doi.org/10.1016/j.jfca.2025.107915

[9] Ajikumar, P. K., Shilpashree, N. H., Manoj, P., Gondaliya, N., Pradhan, A., & Pandiselvam, R. (2025). Raman spectroscopy coupled with machine learning for rapid detection of coconut oil adulteration. Journal of Food Measurement and Characterization, 19, 815-830. https://doi.org/10.1007/s11694-024-02907-9

[10] Horns, C., Kuchta, M., Prevolnik, M., Ogrinc, N., & Petrakis, E. A. (2025). Spatially offset Raman spectroscopy for sustainable olive oil authentication in unopened dark glass bottles. Food Control, 177, 111389. https://doi.org/10.1016/j.foodcont.2025.111389

[11] Chen, Y., Chu, B., Luo, J., Ouyang, Q., Zhan, H., Chen, X., Xing, B., Yang, X., & Sun, C. (2026). Rapid identification of olive oil adulteration using machine learning based on key peak features from Raman spectroscopy. npj Science of Food, 10, 94. https://doi.org/10.1038/s41538-026-00525-7

[12] Liang, S., Gan, Z., Ju, X., Gu, H., & Zhang, R. (2025). Qualitative identification and adulteration quantification of extra virgin olive oil with MTDL using a portable Raman spectrometer. Food Analytical Methods, 18(3), 385-397. https://doi.org/10.1007/s12161-024-02728-0

[13] Liang, S., Gao, X., Li, J., Gan, Z., Li, G., Gu, H., & Zhang, R. (2025). Quick and reagent-free monitoring of edible oil saponification values and palm oil acid value using portable Raman spectroscopy. Food Chemistry, 482, 144103. https://doi.org/10.1016/j.foodchem.2025.144103

[14] Wang, D., Song, F., Zhang, Z., Zhang, Z., Wu, D., Chen, X., Cheng, L., & Zhang, Y. (2025). Raman spectroscopy combined with machine learning for rapid identification of aflatoxin-contaminated peanut oil. Food Control, 180, 111737. https://doi.org/10.1016/j.foodcont.2025.111737

[15] Chen, Y., Wang, D., Wang, L., Huang, X., Yang, X., & Sun, C. (2026). Quantitative analysis of beta-carotene and unsaturated fatty acids in blended olive oil by Raman spectroscopy and 2DCOS image residual neural network. Food Chemistry, 484, 142621. https://doi.org/10.1016/j.foodchem.2024.142621

[16] Leng, T., Chen, R., Li, X., Yuan, H., & Wu, J. (2025). Raman spectroscopy and fusion machine learning algorithm for evaluating oxidative stability of Camellia oleifera seed oil. Journal of Food Composition and Analysis, 139, 107191. https://doi.org/10.1016/j.jfca.2025.107191

[17] Adade, S. Y. S. S., Lin, H., Johnson, N. A. N., Nunekpeku, X., Ekumah, J.-N., Kwadzokpui, B. A., Li, H., Agyekum, A. A., & Chen, Q. (2026). Machine learning-assisted Raman spectroscopy for non-destructive analysis of crude palm oil quality. npj Science of Food, 10, 77. https://doi.org/10.1038/s41538-026-00503-z

[18] Rios-Reina, R., Dorado, G., Sanchez, F. J., & Garcia-Gonzalez, D. L. (2024). A comparative study of fluorescence, UV-visible, FTIR and Raman spectroscopies combined with multivariate analysis for the classification of extra virgin and virgin olive oils. Talanta, 279, 126581. https://doi.org/10.1016/j.talanta.2024.126581

[19] Bandiera, V. S., Marengo, E., Manfredi, M., Marengo, A., & Robotti, E. (2025). Comparing deep and classical chemometrics on fused HPLC and NMR data for the detection and characterization of EVOO adulteration. Food Chemistry, 472, 142915. https://doi.org/10.1016/j.foodchem.2025.142915

[20] Alharbi, M. H., Sedman, J., & Ismail, A. A. (2025). The detection of adulteration of olive oil with various vegetable oils and animal fats using 700 MHz NMR spectroscopy. European Journal of Lipid Science and Technology, 127(4), 2400188. https://doi.org/10.1002/ejlt.202400188

[21] Hashempour-Baltork, F., Khosravi-Darani, K., Hosseini, H., Farshi, P., & Reihani, S. F. S. (2024). Recent methods in detection of olive oil adulteration: State-of-the-art. Journal of Agriculture and Food Research, 16, 101123. https://doi.org/10.1016/j.jafr.2024.101123

[22] Singh, D., Sharma, R., Shivanna, S. K., Gandhi, K., Singh, R., & Sharda, T. (2025). Detection of adulteration in ghee using Raman spectroscopy in combination with chemometrics. Food Control, 178, 111481. https://doi.org/10.1016/j.foodcont.2025.111481

[23] Goyal, R., Singha, P., & Singh, S. K. (2024). Spectroscopic food adulteration detection using machine learning: Current challenges and future prospects. Trends in Food Science & Technology, 146, 104377. https://doi.org/10.1016/j.tifs.2024.104377

[24] Shi, S., Zhang, K., Tian, N., Jin, Z., Liu, K., Huang, L., Tian, X., Cao, C., Zhang, Y., & Jiang, Y. (2025). Spectroscopic techniques combined with chemometrics for rapid detection of food adulteration: Applications, perspectives, and challenges. Food Research International, 211, 116459. https://doi.org/10.1016/j.foodres.2025.116459

[25] He, W., & Zeng, Q. (2025). Non-invasive food authentication using vibrational spectroscopy techniques for low-resolution food fingerprinting. Applied Sciences, 15(11), 5948. https://doi.org/10.3390/app15115948

[26] Lun, R., Sun, J., Li, S., Yang, J., & Zhu, Z. (2025). Deep learning-enhanced spectroscopic technologies for food quality assessment: A review. Critical Reviews in Food Science and Nutrition, 65(27), 6313-6333. https://doi.org/10.1080/10408398.2024.2371283

[27] Kolasinac, S. M., Kantar, S., Dimic, I., Bursac Kovacevic, D., Putnik, P., Pavlic, B., & Pintać, D. (2025). Spectroscopic approach in determination of carotenoids and chlorophylls in pumpkin seed oils with different origins. Foods, 14(10), 1784. https://doi.org/10.3390/foods14101784

[28] Zhao, Y., Ni, X., & Tang, M. (2025). Feature selection-driven machine learning for parallel species authentication and adulteration quantification in commercial dairy products via Raman fingerprints. LWT, 238, 118839. https://doi.org/10.1016/j.lwt.2025.118839

[29] Sun, J., Cai, J., Wang, X., Ma, T., Hu, Z., & Zhang, J. (2025). Raman spectroscopy powered by machine learning methods for rapid identification of foodborne pathogens. Food Bioscience, 65, 105915. https://doi.org/10.1016/j.fbio.2024.105915

[30] Luo, N., Xu, D., Xing, B., Yang, X., & Sun, C. (2024). Principles and applications of convolutional neural network for spectral analysis in food quality evaluation: A review. Journal of Food Composition and Analysis, 128, 105996. https://doi.org/10.1016/j.jfca.2024.105996